An Experimental Investigation of Blade-Vortex Interaction at Normal Incidence

Ali R. Ahmadi*
Bolt Beranek and Newman Inc., Cambridge, Massachusetts

Blade-vortex interaction (BVI) near and away from the blade tip was experimentally investigated for normal incidence where the vortex is generally parallel to the rotor axis. The experiment was designed to be representative of the chopping of helicopter main rotor tip vortices by the tail rotor. Tip Mach number, radial BVI station, and freestream velocity were varied. Fluctuating blade pressures, far-field sound pressure level and directivity, velocity field of the vortex, and BVI angles were measured. BVI produced impulsive noise and impulsive pressures near the blade leading edge. The radiation pattern for BVI away from the tip was that of a dipole, with the direction of minimum radiation, previously found to be in the plane of the blade, rotated considerably in the direction of negative angle of attack. This is believed to be due to unsteady drag radiation caused by stronger BVIs in the present study. For BVI near the tip, the intensity of the interaction was reduced and the radiation pattern was more complex. Away from the tip, the peak amplitude of fluctuating pressure on the suction side of the blade (near the leading edge) was larger than that on the pressure side, as expected due to the effect of compressibility. This trend was reversed near the tip.

Nomenclature

b	= number of rotor blades
c	= rotor chord length
c_W	= vortex generator chord length
C_T	= rotor thrust coefficient
d	= vortex core diameter
h	= vortex generator tip/rotor tip vertical separation distance, positive for vortex generator tip outside rotor disk
M_T	= rotor tip Mach number
$p_{B,F}$	= fluctuating component of blade surface pressure
r/c_W	= radial distrance normalized with vortex generator chord
r/R	= radial distance normalized with rotor radius
r_I/R	= radial blade-vortex interaction station normalized with rotor radius
R	= rotor radius
SPL	= sound pressure level, dB re 20 μPa
T	= total rotor thrust
v_i	= induced velocity at rotor disk
v_θ	= vortex azimuthal velocity
V_T	= rotor tip speed
U_∞, V_∞	= components of freestream velocity parallel to rotor axis and rotor disk, respectively
α_W	= vortex generator geometric angle of attack
Γ	= tip vortex circulation
θ	= microphone position, Fig. 1a
λ	= rotor inflow ratio
μ	= advance ratio
Ω	= rotor radian frequency
$(\bar{\ })$	= ensemble-averaged quantity

Presented as Paper 85-0003 at the AIAA 23rd Aerospace Sciences Meeting, Reno, NV, Jan. 14-17, 1985; received Feb. 1, 1985; revision received Aug. 23, 1985.

*Scientist; currently, Associate Professor, Department of Aerospace Engineering, California State Polytechnic University, Pomona, CA. Member AIAA.

Introduction

ONE of the main causes of helicopter impulsive noise is blade-vortex interaction(BVI), which also causes high unsteady loads at the blades.[1] For the main rotor, BVI occurs when a blade passes close to a (main rotor) trailing vortex which is generally parallel to the plane of blade motion. For the tail rotor, the significant BVI occurs when the main rotor tip vortices pass through the tail rotor disk—a situation that exists under most flight conditions. Here, the vortices are generally perpendicular to the rotor disk and are chopped by the blades: "BVI at normal incidence." This main rotor/tail rotor interaction has been studied experimentally by a few investigators[2-4] who found an increase in tail rotor noise due to the interaction.

The only detailed study of noise radiation due to BVI at normal incidence is by Schlinker and Amiet,[5] who developed an aeroacoustic theory (linearized, inviscid, compressible) for a blade of infinite span interacting with a straight vortex at normal incidence. To validate their theory, they conducted an exeriment consisting of an incident tip vortex interacting with a rotor at the radial station $r_I/R = 0.80$ for tip Mach numbers $M_T \leq 0.55$. The theory predicts the sound pressure level (SPL) for the acoustic spectra and directivity patterns to within 5 dB at low frequencies.

The main objective of the present work was to conduct a detailed experimental investigation of noise radiation and fluctuating blade pressures due to BVI at normal incidence near and away from the blade tip. The experiment that used an isolated vortex and a model rotor was designed to isolate BVI noise from other types of rotor noise. Figure 1 shows the configuration of the experiment, where a two-bladed model rotor was operated with its axis parallel to the freestream direction. An isolated tip vortex was generated by an upstream semispan wing (vortex generator) convected downstream and ingested by the rotor.

Choice of this simplified configuration was motivated primarily by a desire to isolate and study in detail BVI at normal incidence. To ensure that the experiment was representative of the chopping of helicopter main rotor tip vortices by the tail rotor, the relevant similarity parameters for the tail rotor were matched and the model rotor was designed on the basis of a survey of the geometry of two-bladed tail rotors. The experiment does not account for helicopter forward-motion effect (hover condition). However, forward motion of

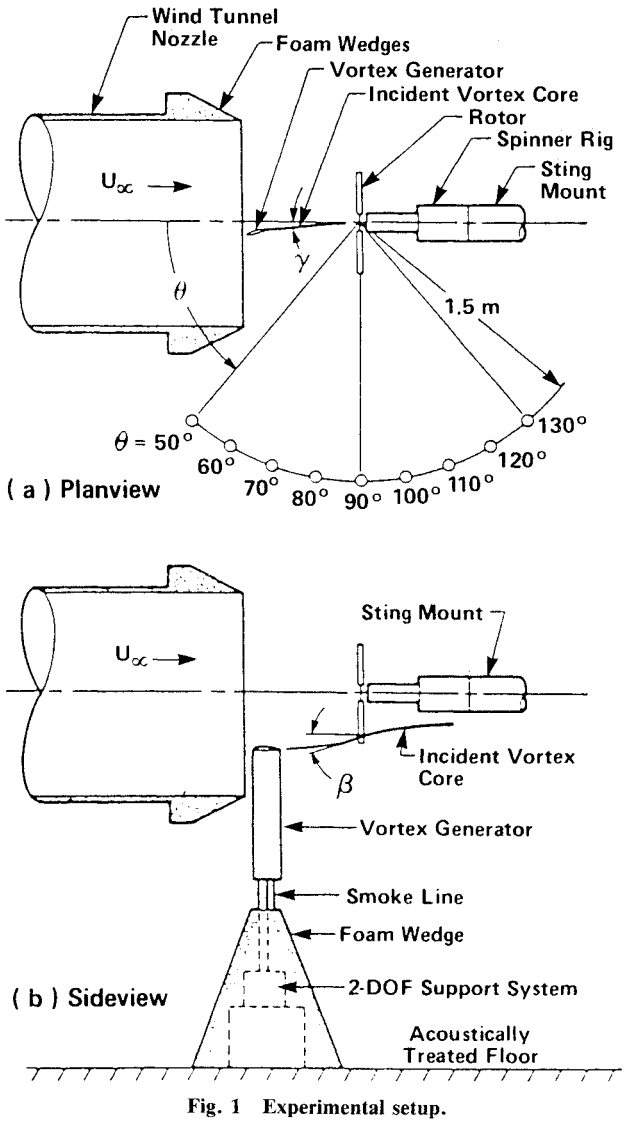

Fig. 1 Experimental setup.

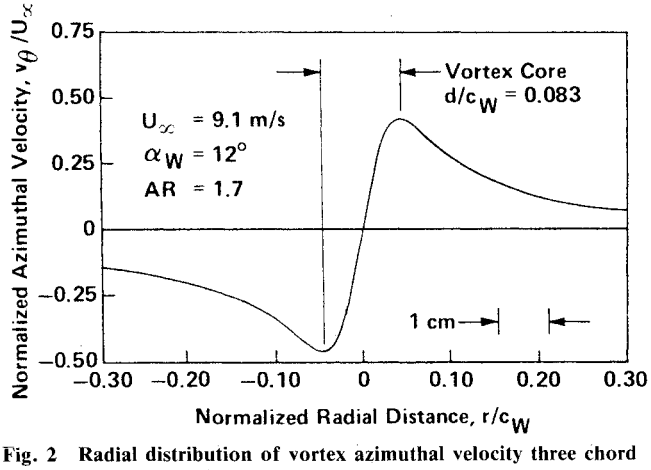

Fig. 2 Radial distribution of vortex azimuthal velocity three chord lengths downstream of the vortex generator.

the helicopter may not significantly affect the present results, since it primarily shifts the position of the main rotor wake as it passes over the tail rotor disk.

The key parameters varied during the tests were tip Mach number M_T, radial BVI station r_I/R, and freestream velocity U_∞. An array of nine microphones located on a horizontal circular arc (Fig. 1) measured the far-field SPL and directivity of the resulting impulsive noise. Four miniature blade-mounted pressure transducers measured the resulting fluctuating

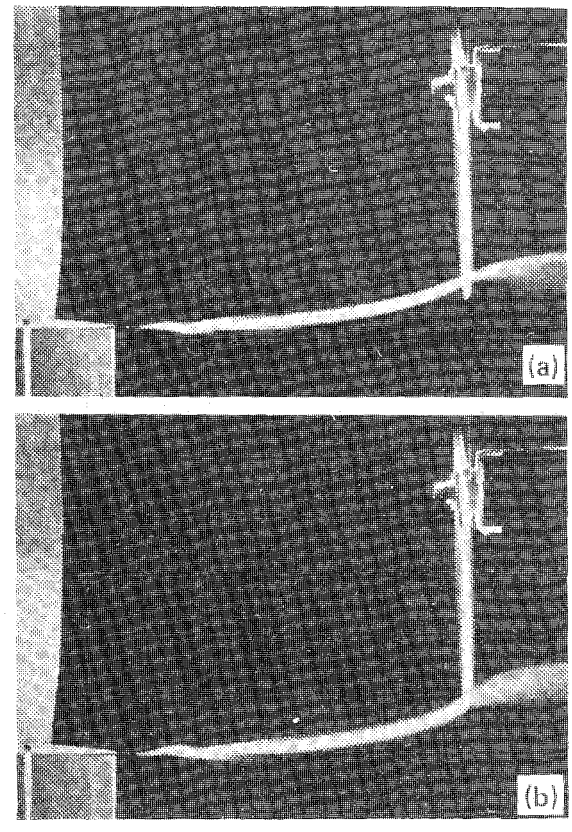

Fig. 3 Flow visualization of BVI for a) test condition 2 and b) test condition 5.

pressures on the blades near the leading edge. The velocity field of the incident vortex was measured with a miniature hot wire. BVI angles were measured by use of flow visualization and photography.

At the present time, no theoretical results are available for comparison with the present measurements where unsteady drag and/or three-dimensional effects must be accounted for. The present results may also be useful in the study of the aeroacoustics of counterrotating and pusher propellers. Additional details of the present work can be found in Ref. 6.

Experimental Approach and Instrumentation

Acoustic Wind Tunnel Facility

The experiments were conducted in the Bolt Beranek and Newman high-speed acoustic wind tunnel, in Cambridge, MA.[7] The tunnel is of the open-jet type with a large anechoic chamber with a cutoff frequency of 160 Hz. The tunnel can achieve a maximum velocity of 46 m/s for the 1.5-m^2 round nozzle used in the tests. The overall turbulence level is 0.23%. The facility is equipped with a rotor spinner rig capable of operating at speeds up to 9000 rpm and equipped with a 16-channel high-speed slip ring.

Model Rotor and Vortex Generator

Rotor Similarity Parameters

In order for the experiment to be representative of the chopping of helicopter main rotor tip vortices by the tail rotor, the following dimensional and nondimensional similarity parameters appropriate to a tail rotor were matched.

1) Rotor tip speed, $V_T = 183$-213 m/s.
2) Advance ratio, $\mu = V_\infty/(\Omega R) = 0$-$0.4$.
3) Blade loading, $C_T/\sigma = 0.1$ max.
4) Disk loading, $T/(\pi R^2) = 239$-479 Pa.
5) Inflow ratio, $\lambda = (U_\infty + v_i)/(\Omega R) = 0.05$-$0.1$ (hover).

Here $C_T = T/[\rho\pi R^2(\Omega R)^2]$ is the rotor thrust coefficient and $\sigma = bc/(\pi R)$ the rotor solidity. In addition, to ensure aerodynamic similarity and to eliminate vortex shedding

noise, boundary-layer trip strips were installed on the suction and pressure sides of the blades. The tripping device consisted of strips of 0.2-mm-thick pinked aluminum tape installed at the quarter-chord position.[8,9]

To match the rotor similarity parameters, rotor thrust was calculated using the extended blade-element theory of Ref. 10 with Prandtl-Betz tip loss correction and Prandtl-Glauert compressibility correction. For test condition 1 (see Table 2), the result was in good agreement with those of the lifting-surface theory of Ref. 11 with a Prandtl-Glauert compressibility correction. The lifting-surface theory was also used to calculate radial blade thrust distribution and rotor torque. For the present test configuration, the advance ratio $\mu = 0$ for all test conditions because $V_\infty = 0$.

Rotor/Vortex Generator Sizing

The relative size of the model rotor and vortex generator was determined from a survey of light helicopters with two-bladed tail rotors. Parameters of interest were tail rotor solidity σ, blade aspect ratio $\mathcal{R}$, and the ratio of main rotor chord to tail rotor chord λ_1. The selected values were approximately the average values from the survey: $\sigma = 0.127$, $\mathcal{R} = 5.00$, and $\lambda_1 = 2.75$. According to the wake roll-up theory of Ref. 12, the wake of the vortex generator is essentially rolled up at a distance $2.5c_W$ downstream of the trailing edge. It is also known that tip vortices of helicopter main rotors roll up faster than those of fixed-wing aircraft. Thus, the model rotor was placed three chord lengths downstream of the vortex generator trailing edge.

Model Rotor

A simple generic model rotor was designed and constructed with the following characteristics: number of blades: 2; diameter: 0.6 m; blade section: NACA 0012; blade planform: rectangular; twist: 0; collective pitch: 9 deg (fixed); chord length: 6.1 cm; blade tip: flat; blade aspect ratio: 5; rotor solidity: 0.127. Constant collective pitch was selected because of the low sensitivity of BVI noise to blade collective pitch.[5]

Vortex Generator

The vortex generator consisted of a semispan wing with the following characteristics: airfoil section: NACA 0012; planform: rectangular; twist: 0; span: 0.8 m; chord: 16.8 cm; tip geometry: NACA 0012 half-body of revolution. The vortex generator was mounted on a support system that allowed it to be moved vertically, to adjust BVI station r_I/R, and to adjust its angle of attack.

To ensure aerodynamic similarity, a boundary-layer trip strip consisting of 0.4-mm-thick pinked aluminum tape was installed at the quarter-chord position on both sides of the vortex generator and around the tip. To check for fully attached flow at all angles of attack, a row of tufts was installed on the suction side near the trailing edge. An internal tube carried the "smoke" to the tip.

Table 1 Location of blade-mounted transducers (BMT)

Transducer	Rotor blade	Blade surface	Radial location, r/R	Chordwise distance from leading edge, x/c
BMT 1	1	Pressure side	0.975	0.10
BMT 2	1	Suction side	0.975	0.10
BMT 3	2	Pressure side	0.90	0.10
BMT 4	2	Suction side	0.90	0.10

Instrumentation

Flowfield Measurements

The velocity field of the incident vortex and the velocity defect in the vortex generator wake were measured at the rotor disk (rotor removed) by the use of a single miniature 45-deg stanted hot wire 5 μm in diameter and 1.22 mm long. The sensor was mounted on a long, slender probe support aligned with the freestream to minimize disturbances to the vortex. The probe was traversed (0.85 mm/s) through the flowfield twice with a rotation of 180 deg. The two components of velocity at each point are then obtained from the sum and difference of the mean linearized voltages of the sensor for the two orientations.

Acoustic Measurements

Far-field SPL and directivity of BVI were measured by an array of nine 1.27-cm B&K microphones mounted at grazing incidence on a horizontal circular arc of 1.5 m radius centered at the rotor center (Fig. 1). The microphones, which have flat response over the 160 Hz-20 kHz range of the study, were located at 10-deg increments from $\theta = 50$-130 deg. The microphones were located ahead of the blade that chops the vortex, because preliminary measurements showed that BVI noise radiated primarily ahead of the blade.

Fluctuating Blade Pressure Measurements

Four miniature blade-mounted transducers (BMT) measured the fluctuating blade pressures. The BMTs (Kulite Model LQ-5-080) had a sensor area 1 mm in diameter (1.6% of blade chord) and were mounted in pairs on opposite sides of the blades. Guided by the full-scale unsteady blade pressure data of Ref. 13, the BMTs were located as close to the leading edge as possible: 10% of chord from the leading edge. One pair of BMTs was located at $r/R = 0.90$ on one blade and the other pair at $r/R = 0.975$ on the other, corresponding to the two BVI stations investigated. BMT designations are listed in Table 1. To ensure accurate measurement of BVI-induced pressures, the BMTs were flush-mounted and strain-isolated from the blades per manufacturer's directions (see also Ref. 14). A dynamic calibration of 144 dB at 250 Hz was applied to the BMTs on the blades, so as to have complete system calibration. The BMT data were analyzed up to 20 kHz, which is about one-tenth of the first resonant frequency of the BMTs.

Data Processing and Analysis

Microphone and BMT signals were amplified and recorded on magnetic tape. The dynamic response of the FM tape

Table 2 Test conditions

Test condition	r_I/R	M_T	U_∞, m/s	α_W, deg	β, deg	γ, deg	$\frac{\Gamma}{2\pi c_W U_\infty}$	d/c_W	h/R
1	0.90	0.55	9.1	12/0	20	3	0.018	0.083	0
2	0.90	0.59	8.2	13.3/0	23	3	(0.018)	—	0.05
3	0.90	0.63	7.3	15/0	35	3	(0.018)	—	0.21
4	0.975	0.55	9.1	12/0	25	3	0.018	0.083	0.12
5	0.975	0.59	8.2	13.3/0	30	3	(0.018)	—	0.15
6	0.975	0.63	7.3	15/0	39	3	(0.018)	—	0.25

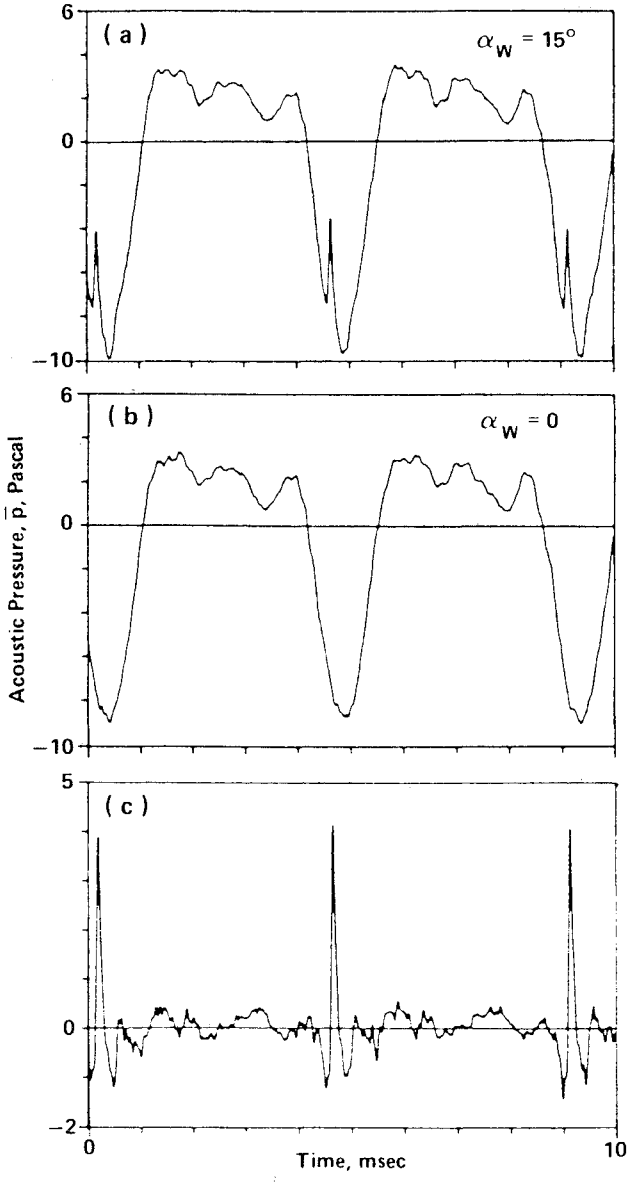

Fig. 4 a,b) Acoustic waveforms and c) BVI signature for test condition 3, $\theta = 50$ deg.

recorder was flat over the 160 Hz-20 kHz range of interest. Acoustic and blade pressure waveforms were ensemble-averaged using a dual-channel analyzer with a resolution of 512 lines. The acoustic waveforms were ensemble-averaged over a time window of 10 ms with a time increment between digital samples of 19.5 μs, ensuring good resolution. For the blade pressure data, the time window was 20 ms and the time increment was 39.1 μs. All ensemble averages were obtained from 50 consecutive samples, with the rotor spinner tachometer signal used as the trigger. Acoustic and blade pressure data were analyzed using a spectrum analyzer with a resolution of 400 lines, at constant bandwidth.

Flow Visualization and Photography

Radial BVI station r_I/R and blade-vortex interaction angles β and γ were set and measured by use of flow visualization and photography. To visualize the flow, oil vapor was injected through a thin tube (1.6 mm diameter) at the wingtip into the evolving vortex core, where it tends to stay confined. Flow visualization of BVI was recorded by two Hasselblad cameras positioned in the rotor disk, one with horizontal and the other with vertical line of sight.

Test Program

Selection of Test Conditions

The strength of BVI is primarily determined by: tip Mach number M_T, BVI angles β and γ, radial interaction station r_I/R, and vortex strength and core size. In the study, the first three of these parameters were varied, while the vortex strength was maintained nearly constant. (Vortex core diameter increased with increasing angle of attack.) The study focused on BVI at two radial stations: $r_I/R = 0.90$ and 0.975. The first is the radial station of maximum spanwise loading for the rotor, as determined from lifting-surface theory.[11] The other is the one for which the vortex core is just inboard of the tip. Three tip Mach numbers were selected for the tests: $M_T = 0.55$, 0.59, and 0.63. Blade-vortex interaction noise for $M_T \leq 0.55$ was studied in Ref. 5. For $M_T > 0.63$, thickness noise and transonic effects prevent isolation of BVI phenomenon.[15,16]

To create strong BVIs, simultaneous with increasing tip Mach number, freestream velocity was reduced from $U_\infty = 9.1$, 8.2, to 7.3 m/s to increase the rotor slipstream contraction and, hence, β. To maintain the vortex strength at approximately the same value, the vortex generator angle of attack was increased simultaneously from $\alpha_W = 12$, 13.3, to 15 deg. The necessary incremental changes in angle of attack were calculated from two-dimensional airfoil theory applied at a section away from the tip. This is justified because 1) all trailing vorticity outboard of the section of maximum loading rolls up to form the tip vortex and 2) the trailing wake is essentially rolled up three chord lengths downstream of the vortex generator trailing edge where the rotor is located. The test conditions are summarized in Table 2.

Qualification Tests

The following qualification tests were conducted in conjunction with the tests.

1) Anechoic Test Environment: This verified that the test environment was anechoic down to 160 Hz.

2) Background Noise: Background noise was measured with the rotor and vortex generator removed but the wind tunnel and rotor spinner operating and generally found to be 20 dB below the rotor noise level.

3) Shear-Layer Injestion: A simplified analysis prior to and flow visualization during the tests were used to insure that the free jet turbulent shear layer was not injested by the rotor.

4) Steadiness of the Tests: Data analysis "experiments" demonstrated the steadiness of rotor rotation rate, freestream velocity, and vortex position and characteristics. The effect of shear-layer refraction and scattering of sound for the present tests was insignificant since the freestream Mach number was below 0.1.[17]

Experimental Results and Discussion

Vortex Flowfield Measurements

Figure 2 shows the azimuthal velocity field of the vortex (data filtered) for test condition 1. The maximum azimuthal velocity is about $0.45U_\infty$, and the diameter of the viscous core is $0.083c_W$. The asymmetry in the velocity distribution is due to the rollup of the trailing vortex sheet. The axial velocity distribution through the vortex center displayed a maximum velocity defect of $0.07V_\infty$, which is not significant. The velocity field of the incident vortex was not measured for the other two test conditions. However, the preceding measurements are expected to be representative of the other test conditions as well, since the strength of the tip vortex was kept nearly constant for all test conditions, as pointed out previously. Flow-visualization results indicate that the vortex core diameter increased with α_W (while U_∞ was reduced). The axial velocity defect in the wake of the vortex generator at zero angle of attack at a spanwise station $0.15c_W$ inboard of the tip was $0.12U_\infty$ max. At nonzero angles of attack, this velocity defect and the width of the wake would be somewhat larger.

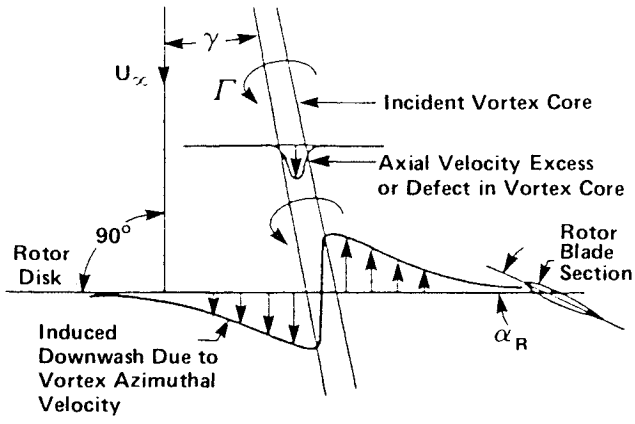

Fig. 5 BVI at normal incidence.

Effect of Rotor Slipstream Contraction

A simplified analysis based on Kelvin's theorem and the continuity equation shows that flow contraction 1) reduces the core diameter in proportion to the flow contraction ratio, and 2) increases the axial velocity in the core in proportion to the inverse square of the contraction ratio. The product of vortex core radius and maximum aximuthal velocity (i.e., circulation) remains constant. Thus, for test condition 2, flow contraction reduces vortex core diameter by 14%, which tends to make the interaction somewhat more impulsive and increases the vortex core axial velocity by 36%. However, since the axial flow velocity outside the core increases by about the same amount, the relative magnitude of the velocity defect in the core remains approximately the same.

Flow-Visualization Results

BVI angles β and γ were measured from photographs of flow visualization of the vortex core. Figure 3 shows two examples for test conditions 2 and 5 in side view. Measured values of β and γ were $=20$-39 deg and ≈ 3 deg, respectively, for all test conditions (Table 2). Because of the small value of γ, the intensity of the BVI depends primarily on β. Since γ is caused by the downwash field of the vortex generator, this suggests that tip vortex strength (and the vortex generator load distribution) were nearly constant at the three sets of α_W and U_∞, as pointed out earlier. Figure 3b shows an apparent enlargement of the vortex core downstream of the rotor disk. This phenomenon was observed for most test conditions. A recent computational study[18] of two-dimensional BVI at low Reynolds number has shown vortex core enlargement (diffusion) due to BVI; a phenomenon not well understood. The apparent core enlargement in Fig. 3b is believed to be due to action of centrifugal forces on "smoke" particles entrained into rotor blade boundary layer, because the enlargement is primarily radially outward. That is, it probably does not represent actual vortex core enlargement.

Far-Field SPL and BVI Signatures

Rotor acoustic waveforms for vortex-present ($\alpha_W > 0$) and vortex-absent ($\alpha_W = 0$) cases were ensemble-averaged. An example is shown in Fig. 4, where it is seen that the vortex creates an impulsive feature in the waveform. To obtain the net effect of the vortex (BVI signature), the waveform for the vortex-absent case was subtracted from that for the vortex-present case to remove the rotor loading noise and that due to vortex generator viscous wake. The impulsive character and shape of the resulting BVI signature (Fig. 4c) are in qualitative agreement with the time-domain calculations of Ref. 19 for a blade cutting through the center of a turbulent vortex (where the vortex-induced downwash field is similar to the present one, see Fig. 5) and the qualitative predictions of Ref. 1 (based on the Ffowcs-Williams and Hawkins formulation) for nonintersecting parallel BVI. The present results thus show no significant additional effect due to the chopping of the vortex core. However, the results are expected to be significantly affected in the presence of large axial velocity in the core.

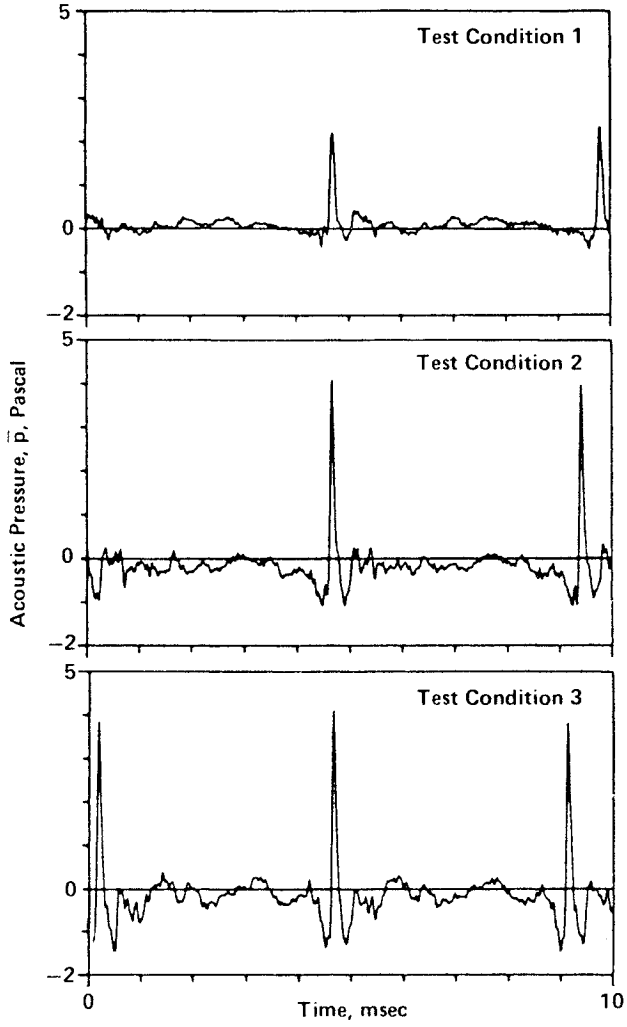

Fig. 6 BVI signature for $\theta = 50$ deg for three different test conditions, $r_I/R = 0.90$

Figure 6 shows a comparison of BVI signatures at $\theta = 50$ deg for test conditions 1-3, $r_I/R = 0.90$. As expected, the peak amplitude of the BVI signature increases with increasing M_T and β (Table 2), indicating stronger BVIs. Similar results were obtained for test conditions 4-6, $r_I/R = 0.975$, except all peak amplitudes were smaller than their counterparts for $r_I/R = 0.90$. This is due to a three-dimensional (3-D) relief effect near the rotor tip which reduces the intensity of BVI radiation. Figure 7 shows the radiation pattern of BVI signatures ($\theta = 60$, 100, and 130 deg) for test condition 2. BVI radiation was found to be more intense for those microphone positions farthest removed from the rotor disk, with minimum radiation occurring near $\theta = 100$ deg. The significance of the latter is discussed below.

Rotor Acoustic Spectra

The effect of BVI on the rotor aeroacoustics is also seen from a comparison of rotor acoustic spectra for vortex-present and vortex-absent cases. Figure 8 shows an example for test condition 2, $\theta = 50$ deg. It is seen that BVI significantly alters the rotor spectrum by increasing the rotor tone levels over a wide frequency range. For the conditions tested, BVI generally increased rotor tone levels by 5-15 dB, with the increase extending up to 10-15 kHz. A comparison of the spectra

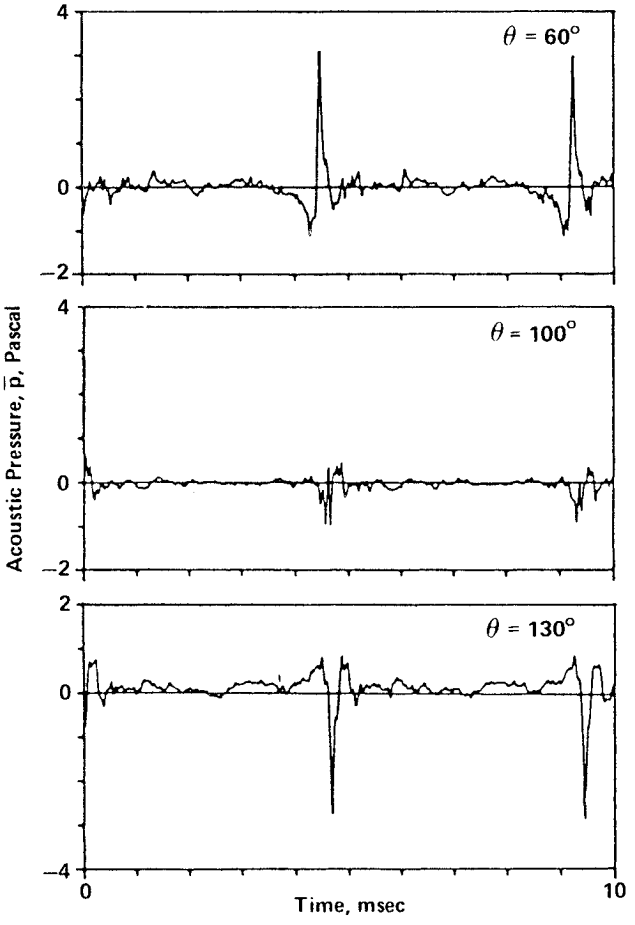

Fig. 7 Radiation pattern of BVI signature for test condition 2.

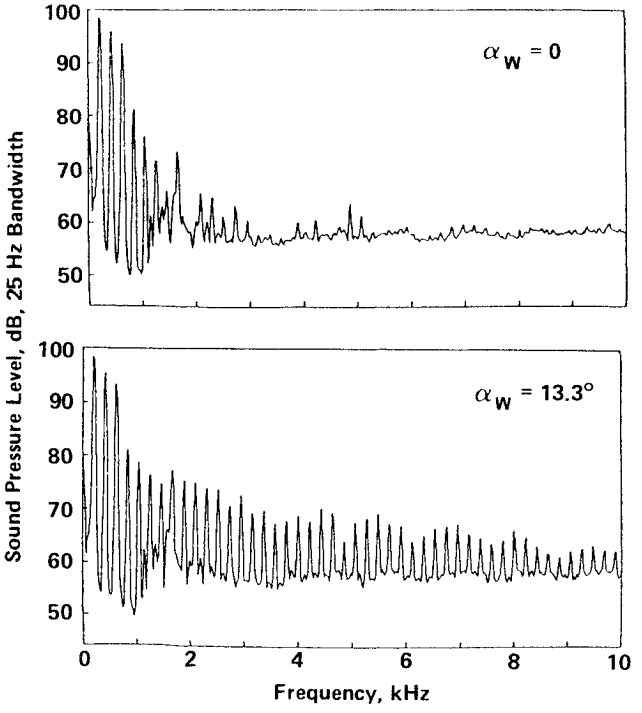

Fig. 8 Effect of BVI on rotor acoustic spectra for test condition 2, $\theta = 50$ deg.

for test conditions 1-3 showed that, with increasing M_T and β, the BVI-induced tone levels were larger and extended to higher frequencies, i.e., stronger BVIs. A similar trend was observed for test conditions 4-6, except these showed weaker BVIs compared with their counterparts at $r_I/R = 0.90$, as explained previously.

Directivity Patterns

BVI directivity patterns were obtained by plotting the measured tone levels as a function of microphone position θ for selected harmonics of the blade passing frequency (BPF). Figure 9 shows the results for test condition 2, for 1, 5, 10, 15, 25 and 35 × BPF harmonics. For each test condition, the first few harmonics are dominated by the rotor loading noise. For BVI away from the tip ($r_I/R = 0.90$), the BVI-induced higher harmonics display a minimum at $\theta = 90$-100 deg, with nearly equal tone levels on either side. For test condition 2, this direction is $\theta \approx 97$ deg. This is also seen in the corresponding radiation pattern of BVI signatures summarized in Fig. 7, where there is a minimum at about $\theta \approx 100$ deg and a polarity reversal about that point at nearly constant amplitude. This demonstrates the dipole character of the radiation. The direction of minimum BVI noise radiation, previously found to be in the plane of the blade (i.e., $\theta = 81$ deg) for interaction farther away from the tip ($r_I/R = 0.80$),[5] is found to be significantly rotated in the negative angle-of-attack direction by about 16 deg. It is shown in the next section that this shift is probably caused by unsteady drag radiation due to stronger BVIs.

For BVI near the tip ($r_I/R = 0.975$), the directivity patterns for the higher harmonics show a more complex radiation pattern with minima occurring between $\theta = 80$-120 deg. This is believed to be due to a more complex source near and diffraction at the tip.

Unsteady Drag Radiation

The shift in the orientation of the BVI dipole radiation pattern (for BVI away from the tip) is believed to be due to unsteady drag dipole radiation caused by stronger BVIs in the present study. It can be shown that unsteady drag dipole radiation combines with unsteady lift dipole radiation (expected to be in phase) to give rise to a rotated dipole radiation pattern, as shown in Fig. 10. The dipole rotation angle $\phi = \tan^{-1}(|\hat{D}|/|\hat{L}|)$, where $|\hat{D}|$ and $|\hat{L}|$ are, respectively, the amplitudes of unsteady drag and lift of the rotor blade section encountering the vortex. For test condition 2, $\phi \approx 16$ deg, which corresponds to $|\hat{D}| \approx 0.3\ |\hat{L}|$—a large amplitude for unsteady drag. Lack of unsteady drag radiation in the measurements of Ref. 5 is believed to be due to weaker BVIs: $M_T \leq 0.55$, $r_I/R = 0.80$, $\beta \leq 14.6$ deg. Also, their theoretical predictions do not account for an unsteady drag effect.

Fluctuating Blade Pressures

Unsteady blade pressure waveforms (steady component removed) were ensemble-averaged for vortex-present and vortex-absent cases (Figs. 11a and 11b, respectively). The net effect of the vortex on the fluctuating blade pressure is obtained from the difference of the two cases (Fig. 11c). It is seen that BVI produces impulsive pressures on the blades near the leading edge. The regular small-amplitude waveforms seen in Figs. 11a and 11b are due to certain blade natural frequencies communicated to the BMT through residual base strain. The frequencies and amplitudes of these for the vortex-present and -absent cases are nearly the same and, hence, cancel each other (Fig. 11c). This was especially true for test conditions 2, 3, 5, and 6 with large M_T and β.

The fluctuating blade pressure at BMT 1 consistently showed the highest peak amplitude for all test conditions. This is due, in part, to the large values of local Mach number and β at this station. Figure 12 shows the fluctuating blade pressure at BMT 1 for test conditions 1-3, where the peak amplitude increases with increasing M_T *and* β. Similar results were obtained for test conditions 4-6, except all peak amplitudes were smaller than their counterparts for $r_I/R = 0.90$ (3-D relief effect).

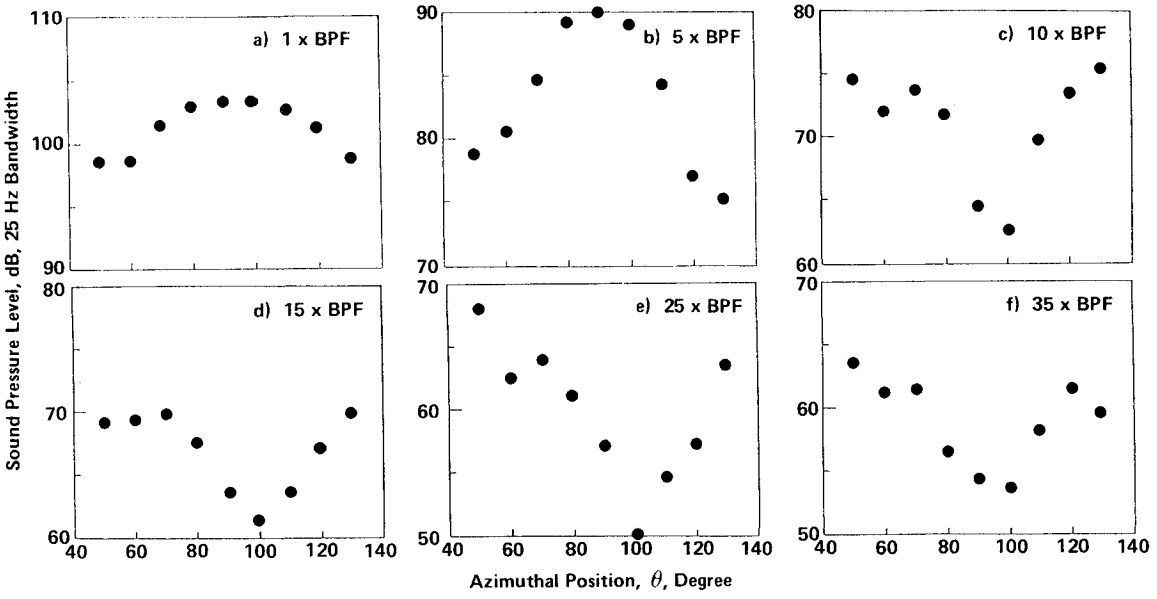

Fig. 9 Directivity pattern of BVI harmonic noise for test condition 2.

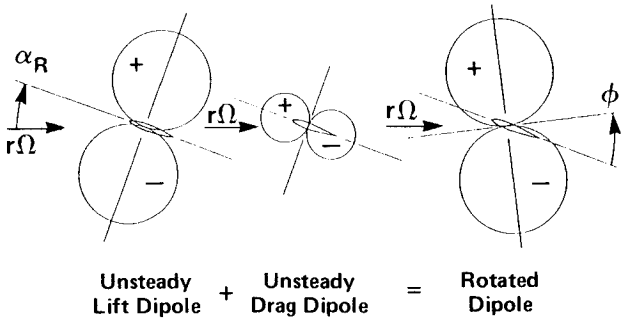

Fig. 10 Effect of unsteady drag dipole radiation in rotating BVI directivity pattern.

For all test conditions, away from the tip, the peak amplitude of fluctuating blade pressure on the suction side was generally larger than that on the pressure side. This is expected because of fluid acceleration and greater compressibility effect on the suction side of the blade, especially near the leading edge. Near the tip, however, this trend was reversed (see Fig. 13). This reversal is believed to be due to large unsteady induced downwash amplitudes which occur in unsteady flow near the tip, see Ref. 20. A similar trend is seen in the full-scale data of Ref. 13, where at stations removed from the tip the peak amplitude of fluctuating blade pressure on the suction side is larger than that on the pressure side. However, as the blade tip is approached the peak amplitudes approach each other. (The station closest to the tip is $r/R=0.955$.) Presumably, at stations closer to the tip, the trend would be reversed, as observed here.

Fluctuating Blade Pressure Spectra

The effect of BVI on blade pressures is also seen from a comparison of fluctuating blade pressure spectra for vortex-present and -absent cases. Figure 14 shows an example for test condition 2 at BMT 1. It is seen that BVI significantly alters the spectrum by increasing the tone levels over a wide frequency range. For the conditions tested, BVI generally increased the tone levels 10-15 dB extending up to 5-10 kHz. The unusually high peaks (e.g., at 1.4 and 4.4 kHz) are blade natural frequencies communicated to the BMT through residual base strain.

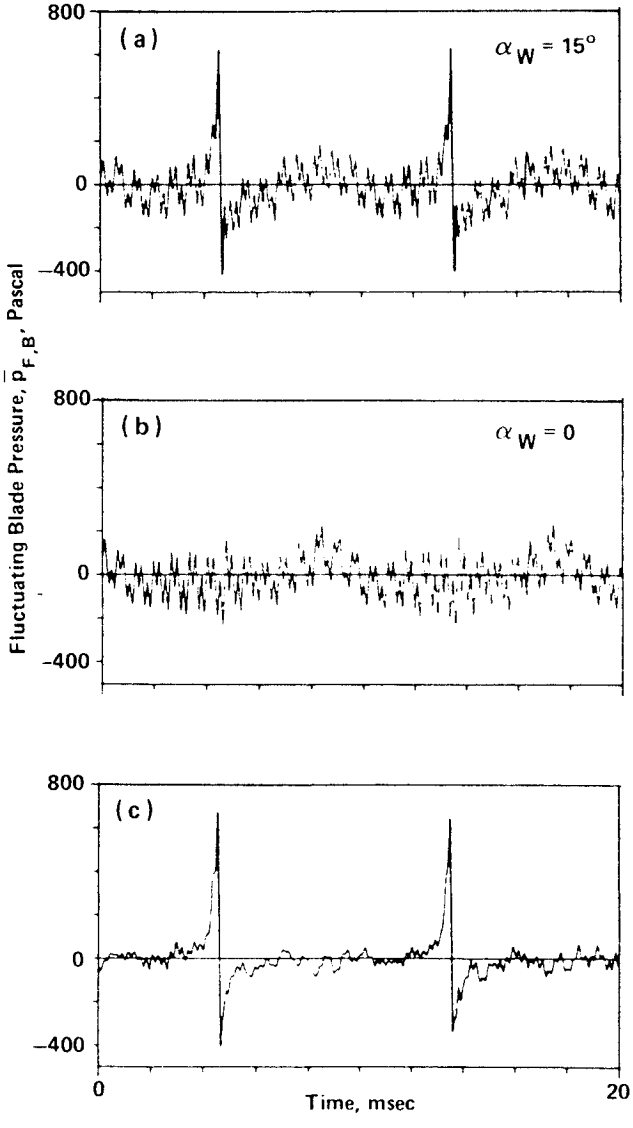

Fig. 11 a,b) Unsteady blade pressure waveforms and c) net fluctuating blade pressure due to BVI for BMT 1, test condition 3.

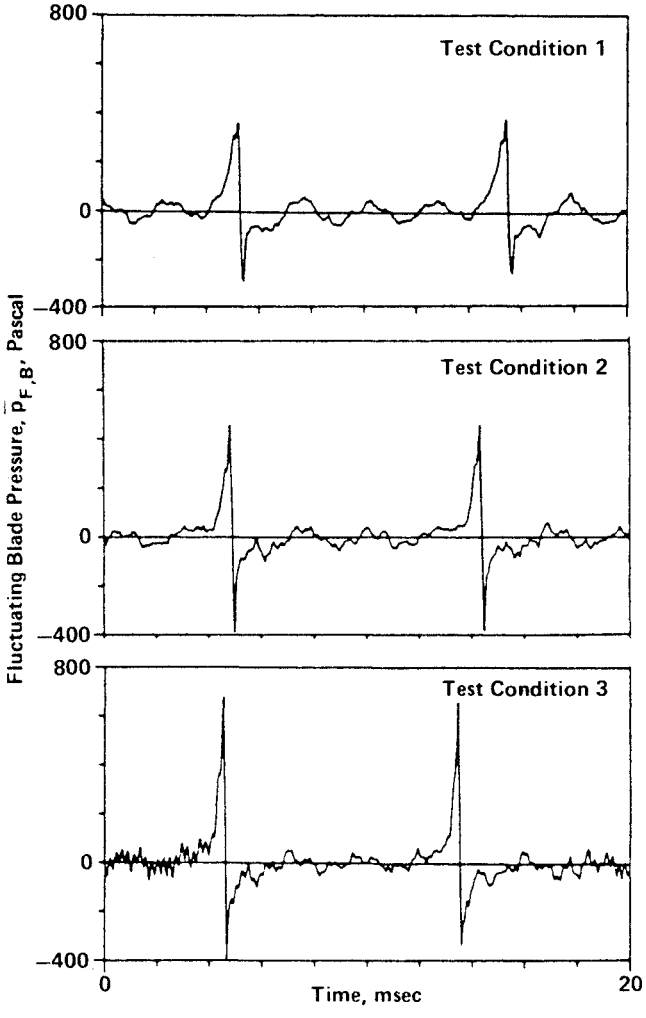

Fig. 12 Fluctuating blade pressure at BMT 1 for three different test conditions, $r_I/R = 0.90$.

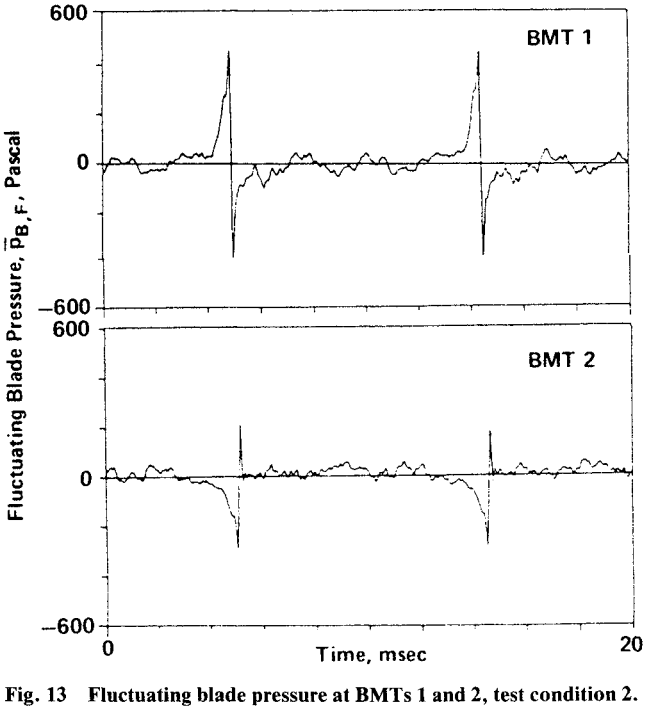

Fig. 13 Fluctuating blade pressure at BMTs 1 and 2, test condition 2.

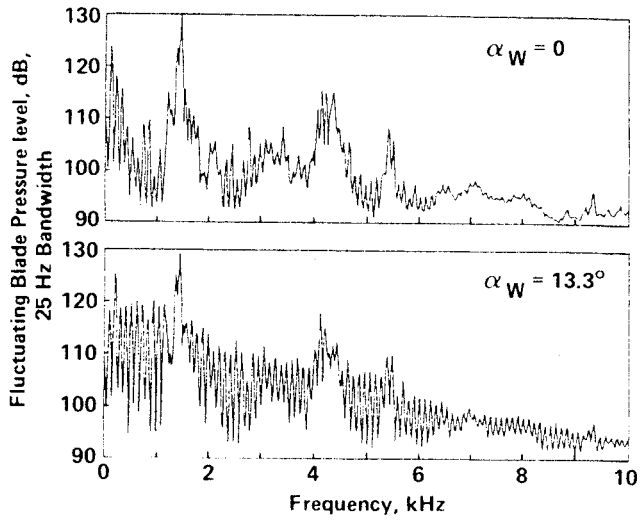

Fig. 14 Effect of BVI on fluctuating blade pressure spectra for test condition 2, BMT 1.

Conclusions and Recommendations

Acoustic Radiation

1) Blade-vortex interaction (BVI) produces impulsive noise which radiates primarily ahead of the blade.

2) For BVI away from the tip, the directivity pattern and acoustic signatures demonstrate the dipole character of the radiation. The direction of minimum noise radiation, previously found to be in the plane of the blade, is significantly rotated in the direction of negative angle of attack. This is believed to be due to unsteady drag dipole radiation.

3) For BVI near the tip, the radiation pattern is more complex due to diffraction at and pressure communication around the tip.

4) The effect of BVI on rotor acoustic spectra is to increase rotor tone levles 5-15 dB extending up to 10-15 kHz.

5) BVI at the radial station of maximum blade loading was more intense than that near the blade tip, due to the 3-D relief effect.

6) Present results show no significant additional effect due to the chopping of the incident vortex core.

Fluctuating Blade Pressures

1) BVI produces impulsive pressures on the blades near the leading edge.

2) Away from the tip, the peak amplitude of fluctuating blade pressure on the suction side was generally larger than that on the pressure side, as expected. However, near the tip, this trend was reversed.

3) For all test conditions, the peak fluctuating blade pressure on the pressure side near the tip showed the largest peak amplitude.

4) The effect of BVI on fluctuating blade pressure spectra is to increase tone levels 5-15 dB extending up to 5-10 kHz.

Theory

1) To predict noise radiation due to strong BVI away from the tip, the two-dimensional theory of Ref. 5 should be extended to include the effect of unsteady drag radiation.

2) A first step in predicting BVI aeroacoustics in the immediate vicinity of the tip is to use the 3-D theory of Ref. 21.

Acknowledgment

This work was conducted under NASA Ames Research Center Contract NAS2-11313.

References

[1]Schmitz, F.H. and Yu, Y.H., "Helicopter Impulsive Noise: Theoretical and Experimental Status," NASA TM-84390, 1983.

[2]White, R.P., Balcerak, J.C., and Pegg, R.J., "A Parametric Model Study of the Noise Generated by the Aerodynamic Interaction of the Tail Rotor with the Wake of the Main Rotor," AHS Mid-East Region Symposium of Rotor Technology, Essington, PA, 1976.

[3]Leverton, J.W., Pollard, J.S., and Willis, C.R., "Main Rotor/Tail Rotor Interactions," *Vertica*, Vol. 1, No. 3, 1977, pp. 213-221.

[4]Pegg, R.J. and Shidler, P.A., "Exploratory Wind Tunnel Investigation of the Effect of the Main Rotor Wake on Tail Rotor Noise," NASA CP-2052, Pt. 1, 1978, pp. 205-219.

[5]Schlinker, R.H. and Amiet, R.K., "Tail Rotor Blade-Vortex Interaction Noise," AIAA Paper 83-0720, 1983.

[6]Ahmadi, A.R., "An Experimental Investigation of the Chopping of Helicopter Main Rotor Tip Vortices by the Tail Rotor," NASA CR-177338, 1984.

[7]Kadman, Y. and Hayden, R.E., "Factors in the Design and Performance of Free-Jet Acoustic Wind Tunnels," *Progress in Astronautics and Aeronautics*, Vol. 46, 1976, pp. 247-258.

[8]Hama, F.R., "An Efficient Tripping Device," *Journal of the Aeronautical Sciences*, Vol. 24, March 1957, pp. 236-237.

[9]Paterson, R.W. and Amiet, R.K., "Noise of a Model Helicopter Rotro Due to Injestion of Turbulence," NASA CR-3213, 1979.

[10]Gessow, A. and Myers, G.C. Jr., *Aerodynamics of the Helicopter*, Ungar Publishing Co., New York, 1952.

[11]Greeley, D.S. and Kerwin, J.W., "Numerical Methods for Propeller Design and Analysis in Steady Flow," *SNAME Transactions*, Vol. 90, 1982, pp. 415-453.

[12]Spreiter, J.R. and Sacks, A.H., "The Rolling Up of the Trailing Vortex Sheet and Its Effect on the Downwash Behind Wings," *Journal of the Aeronautical Sciences*, Jan. 1951.

[13]Shockey, G.A., Williamson, T.W., and Cox, C.R., "AH-1G Helicopter Aerodynamic and Structural Loads Survey," USAAMRDL-TR-76-39, Feb. 1977.

[14]Englund, D.R., Grant, H.P., and Lanati, G.A., "Measuring Unsteady Pressure on Rotating Compressor Blades," NASA TM-79159, 1979.

[15]Schlichting, H. and Truckenbrodt, E., *Aerodynamics of the Airplane*, McGraw-Hill Book Co., New York, 1979.

[16]Abbott, I.H. and von Doenhoff, A.E., *Theory of Wing Sections*, Dover Publications, New York, 1959.

[17]Schlinker, R.H. and Amiet, R.K., "Shear Layer Refraction and Scattering of Sound," AIAA Paper 80-0973, 1980.

[18]Hardin, J.C. and Lamkin, S.L., "Aeroacoustic Interaction of a Distributed Vortex with a Lifting Joukowski Airfoil," AIAA Paper 84-2287, 1984.

[19]Lee, D.J. and Roberts, L., "Interaction of a Turbulent Vortex with a Lifting Surface," AIAA Paper 85-0004, 1985.

[20]Ahmadi, A.R. and Widnall, S.E., "Unsteady lifting-line theory as a singular-perturbation problem," *Journal of Fluid Mechanics*, Vol. 153, 1985, pp. 59-81.

[21]Martinez, R. and Widnall, S.E., "Aerodynamic Theory for Wing with Side Edge Passing Subsonically Through a Gust," *AIAA Journal*, Vol. 21, June 1983, pp. 808-815.